

RESEARCH ARTICLE

Modelling Immunological Effects on Fractional Order of Cholera Dynamics with Behavioral Response via Numerical simulation

Mutairu Kayode Kolawole¹, Atinuke Abidemi Adeniji^{1,*}

¹Department of Mathematical Sciences, Faculty of Basic and Applied Sciences, Osun State University, Osogbo, Nigeria *Corresponding author: atinukeadeniji0@gmail.com

Received: 10 July 2025; Revised: 14 September 2025; Accepted: 19 October 2025; Published: 1 November 2025.

Abstract:

Cholera, caused by *Vibrio cholerae*, remains a persistent public health challenge, particularly in regions with inadequate sanitation. Its transmission dynamics are shaped by host immunity, behavioral responses, and environmental conditions. In this study, we develop a Caputo fractional-order model that integrates immunological effects, hygiene practices, and memory-dependent disease processes to capture the complexity of cholera dynamics. The model incorporates behavioral responses and environmental interactions, providing a more realistic approach for disease analysis. Rigorous mathematical investigations are carried out to establish existence, uniqueness, positivity, and boundedness of solutions. The basic reproduction number is derived to assess thresholds for disease persistence, while the local stability of disease-free and endemic equilibria is analyzed to inform effective control strategies. To approximate solutions of the nonlinear fractional system, we employ the Laplace Adomian Decomposition Method, yielding simulations that align with observed cholera patterns. Results demonstrate that declining immunity accelerates transmission, whereas improved hygiene significantly mitigates outbreaks. This fractional-order approach not only deepens understanding of cholera spread but also offers a robust analytical tool for exploring other infectious diseases with intricate behavioral and immunological dynamics.

Keywords: Mathematical model, Vibrio cholerae, Hygiene, Laplace-Adomian Decomposition Method, Caputo fractional-order, Epidemiological.

1. Introduction

Cholera has not been fully controlled worldwide, as it is especially dangerous among people who have poor access to sanitation. *V. cholerae* research is synthesized in this study, especially focusing on how the bacteria become more virulent, how the immune system responds, improvements in vaccines, and the use of models to study the disease [1]. Even though getting infected provides strong immunity, bestowing immunity for a longer duration is challenging with the existing vaccines [2]. Modeling has an essential role in understanding how cholera is spread and what tools can help to combat it. Reliable predictions about the beginning of outbreaks are more likely when a

fractional-order model with Bayesian neural networks and the Runge-Kutta method is used [3]. A stochastic model combining neural networks and the Adam optimizer is used to study interventions among different populations [4]. A stochastic model that uses the Levenberg-Marquardt algorithm achieves great accuracy when studying infections and environmental changes [5]. With the help of stability and sensitivity analyses, SEIRB frameworks confirm the importance of both treatment and early identification [6]. Modern reviews of studies point out that many of these models are statistical, compartmental, and involve space, advising for the integration of vector-borne cases and accurate estimating of parameters [7]. A Cameroon-based study based on a deterministic SEIRB model reveals spikes in the number of cases happening seasonally and points out the helpfulness of sudden interventions [8]. Reviews highlight that the disease's spread depends on how and when it appears, human behavior, and how data are organized at different scales [9]. Also, it explains that aside from the ill, the early spread is mostly due to people with the virus who have no symptoms [10]. Simulations from SPRI show that keeping fewer people from the protected group to the susceptible group is a good way to manage support actions. Researchers suggest that acting promptly against an epidemic in Haiti results in a quicker recovery [11-13]. Fractal and fractional models are used now, along with the Caputo-Fabrizio derivative, which offer better performance and indicate important factors contributing to virus spread and limitation [14, 15]. They have recently become popular because they model the way diseases with memory act. The Caputo-Fabrizio model pointed out main aspects of vector-borne infections by performing stability and sensitivity analysis [16]. Models that use fractalfractional approaches with decay factors demonstrated the behavior of cholera and how people's memories work [17, 18]. By using decomposition, other fractional methods were able to prove and measure equilibrium behavior and transmission in Ebola and malaria cases [19]. In Sub-Saharan Africa, models for Ebola and malaria also explained the need for quick but long-lasting strategies [20]. Public health campaigns were proven to work in measles infection models and highlight their importance in controlling the disease [21, 22]. Studies on cholera disease also highlighted the immediate but limited effect of treatment and the lasting impact vaccination can have [23]. Using both types of simulations, experts confirmed that using immunization, treatment, and better sanitation helps in eradicating cholera [24, 25]. There are many new cholera outbreaks happening since 2021, mainly in Africa [26]. Many epidemics have taken place in Nigeria due to weak sanitation, poverty, not enough healthcare support, and changes in the climate. Along with laboratory experiments, there is now a stage-switching' model of multidrug-resistant (MDR) cholera, which is supported by both mathematical and numerical analyses [27]. Various studies make it clear that better WASH infrastructure, more vaccination, better surveillance, and safe antibiotic use are needed to stop cholera from spreading and causing deaths [28–31].

2. Methodology

2.1. Model Formulation

The model describes the dynamics of a cholera disease dynamics by integrating a traditional SIRQ model with environmental bacteria and human hygiene efforts. The Susceptible population (S) increases with new births (Λ) and individuals losing immunity (w), while decreasing due to natural death (μ) and infection. The Infected population (I) grows as susceptible become infected and shrinks as individuals are quarantined (δ) , die from the disease (α_1) , or die naturally (μ) . The Quarantined population (Q) is a temporary state for infected individuals, increasing with quarantines and decreasing as people recover (ξ) , die in quarantine (α_2) , or die naturally. The Recovered population (R) grows from recovering quarantined individuals and declines as people lose immunity or die naturally. The environmental Bacteria concentration (B) increases through natural growth (r) and shedding by infected individuals (η) , while decreasing due to hygiene efforts (λ_1) and natural bacterial death (d). Finally, Hygiene efforts (H) are modeled as a resource that increases at a constant rate

 (ρ) and decays over time (α) . This comprehensive model captures the complex interplay between population dynamics, environmental factors, and public health interventions.

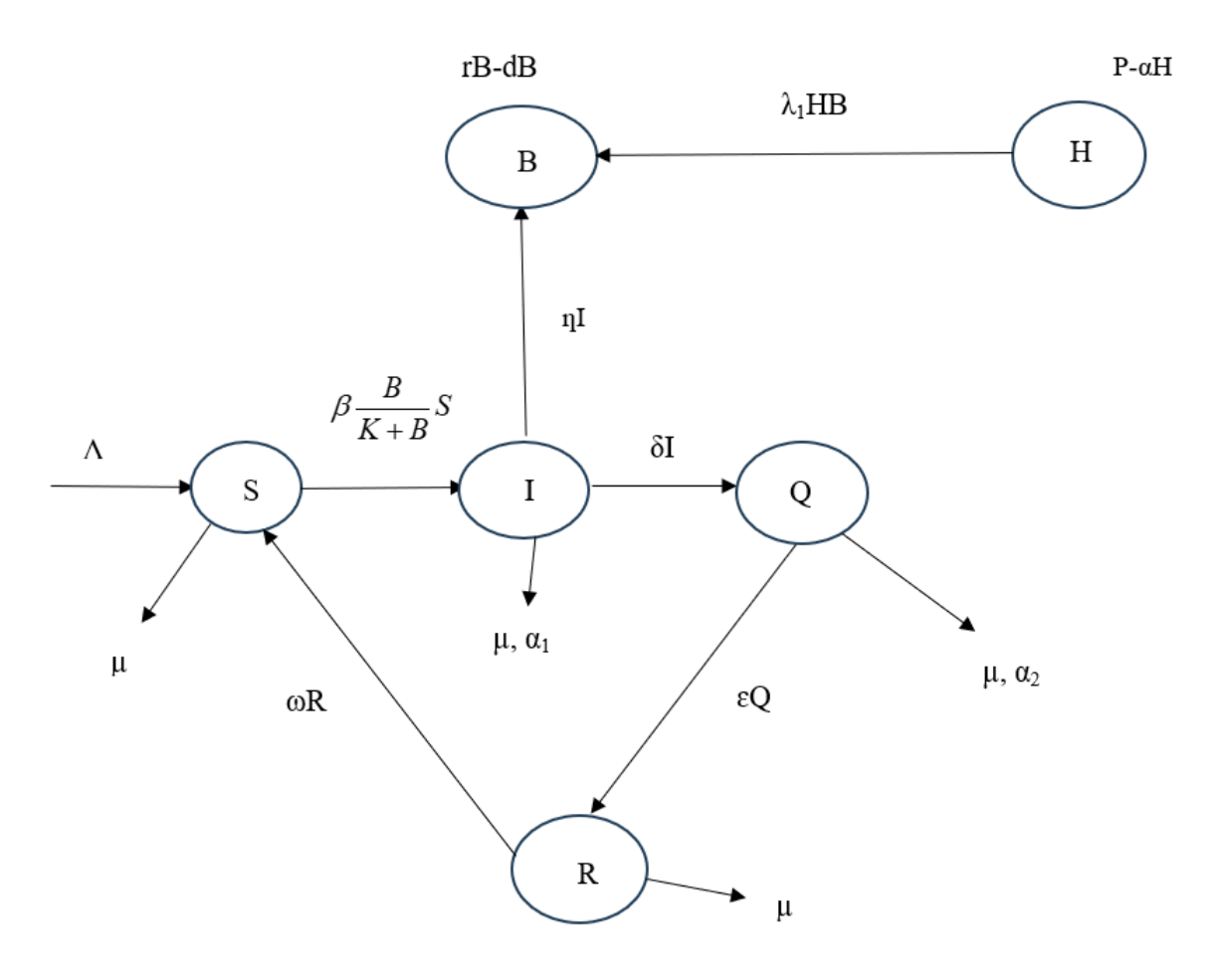


Figure 2.1: Schematic flow of distribution

Modified Model

$$\frac{dS}{dt} = \Lambda - \frac{\beta B(t)S(t)}{K + B(t)} + wR(t) - \mu S(t),$$

$$\frac{dI}{dt} = \frac{\beta B(t)S(t)}{K + B(t)} - (\delta + \alpha_1 + \mu)I(t),$$

$$\frac{dQ}{dt} = \delta I(t) - (\xi + \alpha_2 + \mu)Q(t),$$

$$\frac{dR}{dt} = \xi Q(t) - (w + \mu)R(t),$$

$$\frac{dB}{dt} = rB(t) + \eta I(t) - \lambda_i H(t)B(t) - dB(t),$$

$$\frac{dH}{dt} = \rho - \alpha H(t).$$
(2.1)

For simplicity, let the force of infection be constant such that

$$\lambda = \frac{\beta}{K + B(t)}$$

Now, using the Caputo derivative to reformat the classical derivative in 2.1 to get the following system of fractional ODEs;

$${}^{C}F^{Z}S(t) = \Lambda - \lambda B(t)S(t) + wR(t) - \mu S(t)$$

$${}^{C}F^{Z}I(t) = \lambda B(t)S(t) - (\delta + \alpha_{1} + \mu)I(t)$$

$${}^{C}F^{Z}Q(t) = \delta I(t) - (\xi + \alpha_{2} + \mu)Q(t)$$

$${}^{C}F^{Z}R(t) = \xi Q(t) - (w + \mu)R(t)$$

$${}^{C}F^{Z}B(t) = rB(t) + \eta I(t) - \lambda_{i}H(t)B(t) - dB(t)$$

$${}^{C}F^{Z}H(t) = \rho - \alpha H(t)$$

$$(2.2)$$

Table 2.1: Variable and Parameters Definition

Symbols	Definitions
S(t)	Susceptible Population
I(t)	Infected Population
Q(t)	Quarantined Population
R(t)	Recovered Population
B(t)	Bacteria Concentration
H(t)	Hygiene Efforts
K	Half Saturation Constant
Λ	Recruitment rate
β	Ingestion rate
w	Immunity waning rate
μ	Natural Death
δ	Quarantine rate
α_1	Death rate (Infected)
ξ	Recovery rate
α_2	Death rate (Quarantine)
r	Natural Growth of Bacteria
η	Shedding rate
λ_1	Rate at which Human efforts reduce Bacteria Concentration
d	Bacteria Death rate
ho	Efforts rate to increase hygiene level
α	Decay rate of Hygiene effort
λ	Force of Infection

2.2. Positivity and Boundedness of Solution

Theorem 2.1. The Solutions X = (S(t), I(t), Q(t), R(t), B and H(t)) of the fractional order model 2.2 are non-negative for all $t \ge 0$, with non-negative initial condition in R^6 .

Proof. We have the variables at $X^1|_{\varepsilon(V)}$

$$\label{eq:continuous} \begin{split} {}^CF^ZS^1(t) &= \Lambda + wR(t) > 0, \\ {}^CF^ZI^1(t) &= \beta B(t)S(t) > 0, \\ {}^CF^ZQ^1(t) &= \delta I(t) > 0, \\ {}^CF^ZR^1(t) &= \varepsilon Q(t) > 0, \\ {}^CF^ZB^1(t) &= \eta I(t) > 0, \\ {}^CF^ZH^1(t) &= \rho > 0. \end{split}$$

Where $\varepsilon(v)=[v(t)=0]$ and $v\in\{S(t),I(t),Q(t),R(t),B(t),H(t)\}$ which exist in R^{6+} . Hence, the model 2.2 has a bounded positive solution.

Theorem 2.2. Let Ω_H be the domain containing the human population group, Ω_B be the domain of pathogen population and Ω_h be the domain of time-dependent rate of hygiene measure, in equation 2.2 to 2.4. Then,

$$\Omega_H = \left\{ S, I, Q, R \in R_+^4 : 0 \le S + I + Q + R \le \frac{\Lambda}{\mu} \right\}$$
 (2.2)

$$\Omega_B = \left[B \in R : 0 \le B \le \frac{\Lambda \alpha \eta}{\mu(\alpha d - \alpha r + \rho \lambda_i)} \right]$$
 (2.3)

and

$$\Omega_h = \left[0 \le h \le \frac{\rho}{\alpha} \right]. \tag{2.4}$$

They are positively invariant.

Proof. From 2.1 the total human population

$$N = S + I + Q + R : \Lambda - \mu(S + I + Q + R)$$

$$\frac{dN}{dt} = \Lambda - \mu N \quad .$$

Solving this linear differential equation at $N(0) = N_0$.

$$N(t) \le \frac{\Lambda}{\mu} + e^{-\mu t} \left(\eta_0 - \frac{\Lambda}{\mu} \right)$$

As $t \to \infty$, $w(t) \le \frac{\Lambda}{\mu}$.

Now

$$\frac{dH}{dt} \le \rho - \alpha H(t), \text{ solving at } H(0) = h_0$$

$$H(t) \le \frac{\rho}{\alpha} + e^{-\alpha t} (h_0 - \frac{\rho}{\alpha}) \text{ at } t \to \infty, H(t) = \frac{\rho}{\alpha}$$

$$\frac{dB}{dt} = rB(t) + \eta I(t) - \lambda_i H(t) B(t) - dB(t)$$

$$\Rightarrow \frac{dB}{dt} = rB(t) + \eta(\frac{\Lambda}{\mu}) - \lambda_i(\frac{\rho}{\Lambda}) - dB(t)$$

Solving this linear differential equation at $B(0) = b_0$,

$$B(t) = \frac{\Lambda \alpha \eta}{\mu(\alpha d - \alpha r + \rho \lambda_i)} + e^{\frac{(\alpha d - \alpha r + \rho \lambda_i)}{\alpha}} (b_0 - \frac{\Lambda \alpha \eta}{\mu(\alpha d - \alpha r)}), \text{ as } t = \infty$$
$$B(t) \le \frac{\Lambda \alpha \eta}{\mu(\alpha d - \alpha r + \rho \lambda_i)}.$$

Thus, three variables are bounded above. Also, since all parameters are positive, N(t), B(t) and H(t) are all positive. Hence, they belong to a positive invariant region.

2.3. Existence and Uniqueness of Solution

In this section, we investigated whether or not the solution to the problem exists and unique. This will help us to know if the model represents a physical problem from equation 2.1. Let,

$$M_{1} = \Lambda - \lambda B(t)S(t) + wR(t) - \mu S(t),$$

$$M_{2} = \lambda B(t)S(t) - (\delta + \alpha_{1} + \mu)I(t),$$

$$M_{3} = \delta I(t) - (\xi + \alpha_{2} + \mu)Q(t),$$

$$M_{4} = \xi Q(t) - (w + \mu)R(t),$$

$$M_{5} = rB(t) + \eta I(t) - \lambda_{i}H(t)B(t) - dB(t),$$

$$M_{6} = \rho - \alpha H(t),$$
(2.5)

Then, taking partial derivative of 2.5 gives below

$$\begin{aligned} \left| \frac{\partial M_1}{\partial S} \right| &= -\lambda B - \mu; \left| \frac{\partial M_1}{\partial I} \right| = 0; \left| \frac{\partial M_1}{\partial Q} \right| = 0; \left| \frac{\partial M_1}{\partial R} \right| = w; \left| \frac{\partial M_1}{\partial B} \right| = 0; \left| \frac{\partial M_1}{\partial H} \right| = 0. \\ \left| \frac{\partial M_2}{\partial S} \right| &= \lambda B; \left| \frac{\partial M_2}{\partial I} \right| = -(\delta + \alpha_1 + \mu); \left| \frac{\partial M_2}{\partial Q} \right| = 0; \left| \frac{\partial M_2}{\partial R} \right| = 0; \left| \frac{\partial M_2}{\partial B} \right| = 0; \left| \frac{\partial M_2}{\partial H} \right| = 0. \\ \left| \frac{\partial M_3}{\partial S} \right| &= 0; \left| \frac{\partial M_3}{\partial I} \right| = \delta; \left| \frac{\partial M_3}{\partial Q} \right| = -(\xi + \alpha_2 + \mu); \left| \frac{\partial M_3}{\partial R} \right| = 0; \left| \frac{\partial M_3}{\partial B} \right| = 0; \left| \frac{\partial M_3}{\partial H} \right| = 0. \\ \left| \frac{\partial M_4}{\partial S} \right| &= 0; \left| \frac{\partial M_4}{\partial I} \right| = 0; \left| \frac{\partial M_4}{\partial Q} \right| = \xi; \left| \frac{\partial M_4}{\partial R} \right| = -(w + \mu); \left| \frac{\partial M_4}{\partial B} \right| = 0; \left| \frac{\partial M_4}{\partial H} \right| = 0. \\ \left| \frac{\partial M_5}{\partial S} \right| &= 0; \left| \frac{\partial M_5}{\partial I} \right| = \eta; \left| \frac{\partial M_5}{\partial Q} \right| = 0 \\ \left| \frac{\partial M_5}{\partial R} \right| &= 0; \left| \frac{\partial M_5}{\partial B} \right| = r - \lambda_i H - d; \left| \frac{\partial M_5}{\partial H} \right| = -\lambda_i B. \\ \left| \frac{\partial M_6}{\partial S} \right| &= 0; \left| \frac{\partial M_6}{\partial I} \right| = 0; \left| \frac{\partial M_6}{\partial Q} \right| = 0 \\ \left| \frac{\partial M_6}{\partial R} \right| &= 0; \left| \frac{\partial M_6}{\partial H} \right| = -\alpha. \end{aligned}$$

Hence, since the partial derivatives exist, the solution to the problem is both continuous and bounded. Consequently, the model accurately represents a physical phenomenon and is well-posed.

2.4. Disease Free Equilibrium

This is a state where a disease is no longer present or prevalent in a population. For the disease-free equilibrium, I=0, B=0, Thus, solving at steady states

Let
$${}^CF^ZS = {}^CF^ZI = {}^CF^ZQ = {}^CF^ZR = {}^CF^ZB = {}^CF^ZH = 0.$$
 $\overset{o}{S} = \overset{o}{I} = \overset{o}{Q} = \overset{o}{R} = \overset{o}{B} = \overset{o}{H} = 0,$

DFE is given by;

$$S = \frac{\Lambda}{\mu}, I = 0, Q = 0, R = 0, B = 0, H = \frac{\rho}{\alpha}.$$

$$E_0 = \left(\frac{\Lambda}{\mu}, 0, 0, 0, 0, and \frac{\rho}{\alpha}\right). \tag{2.6}$$

Equation 2.6 gives disease free equilibrium

2.5. Endemic Equilibrium

This refers to a state in which a disease persists within a population at a relatively stable and low prevalence over time.

At this steady state, $B \neq I \neq O$.

Thus, solving, we obtained

$$S^* = \frac{(\delta + \mu + \alpha_1)(\alpha d - \alpha r - \lambda \rho)}{\alpha \eta \kappa}$$
 (2.7)

$$Q^* = \frac{\delta(\alpha d - \alpha r - \lambda \rho)}{\alpha n}.$$
 (2.8)

$$I^* = \frac{\left[(\Lambda k \eta - (\delta + \mu + \alpha_1)\mu(d - r)(w + \mu) + \delta w \varepsilon k(d - r) \right] \left[\alpha - [\delta k w + \lambda \rho](\delta + \mu + \alpha_1)(w + \mu)\mu \right]}{(\delta + \mu + \alpha_1)(w + \mu)k\alpha\eta}$$
(2.9)

$$R^* = \frac{\varepsilon \delta(\alpha d - \alpha r - \lambda \rho)}{\alpha \eta}.$$
 (2.10)

$$B^* = \frac{I^* \alpha \eta}{(\alpha d - \alpha r - \lambda \rho)} \tag{2.11}$$

$$H^* = \frac{\rho}{\alpha} \tag{2.12}$$

Equation 2.7 to equation 2.12 gives Endemic equilibriums of the model.

2.6. Basic Reproduction Number (R_0)

The basic reproduction number R_0 is defined as the average number of secondary cases generated by a single infective individual in a completely susceptible population. This is calculated using the next-generation matrix method as follows below from equation 2.13 to equation 2.15:

$$R_0 = \sigma(FV^{-1})$$
 such that σ is the spectral radius,

$$F = \begin{bmatrix} f_1 \\ f_2 \\ f_3 \\ f_4 \\ f_5 \\ f_6 \end{bmatrix} = \begin{bmatrix} 0 \\ \lambda SB \\ 0 \\ 0 \\ 0 \\ 0 \end{bmatrix}$$
 (2.13)

$$V = \begin{bmatrix} v_1 \\ v_2 \\ v_3 \\ v_4 \\ v_5 \\ v_6 \end{bmatrix} = \begin{bmatrix} \Lambda + wR - \lambda \beta S - \mu S \\ -(\delta + \mu + \alpha_1)I \\ \delta I - (\varepsilon + \alpha_2 + \mu)Q \\ \varepsilon Q - (w + \mu)R \\ rB + \eta I - \lambda_i HB - dB \\ \rho - \alpha H \end{bmatrix}$$
(2.14)

Hence,
$$R_0 = \frac{\lambda \eta \Lambda \alpha}{\mu (\delta + \mu + \alpha_1)(\alpha d - \alpha r + \lambda \rho)}$$
 (2.16)

Equation 2.16 gives Basic Reproduction Number (R_0)

2.7. Local Stability of Disease-Free Equilibrium

The local stability of the DFE is assessed by linearizing the system of differential equations around the disease-free state and examining the eigenvalues of the Jacobian matrix. If all eigenvalues have negative real parts, the DFE is locally asymptotically stable, meaning that small introductions of the infection will fade over time, and the system will return to its disease-free state. To investigate the local stability of the DFE, we compute the Jacobian matrix of equation 2.17 as follows:

$$J = \begin{bmatrix} -(Bk+\mu) & 0 & 0 & w & -kS & 0 \\ Bk & -(\delta+\mu+\alpha_1) & 0 & 0 & kS & 0 \\ 0 & \delta & -(\varepsilon+\alpha_2+\mu) & 0 & 0 & 0 \\ 0 & 0 & \varepsilon & -(\mu+w) & 0 & 0 \\ 0 & \eta & 0 & 0 & -(H\lambda_i+d+r) & 0 \\ 0 & 0 & 0 & 0 & 0 & -\alpha \end{bmatrix}$$
(2.17)

$$\begin{split} \lambda_1 &= -\alpha_1. \\ \lambda_2 &= -\mu. \\ \lambda_3 &= -D. \\ \lambda_4 &= -C. \\ \lambda_5 &= \frac{-1}{2} [B + E + \delta \sqrt{(B - E)^2 + 4A\eta}]. \\ \lambda_6 &= \frac{-1}{2} [B + E + \sqrt{(B - E)^2 + 4A\eta}]. \end{split}$$

Since all the eigenvalues of the Jacobian matrix evaluated at the disease-free equilibrium have negative real parts, the DFE is locally asymptotically stable. This implies that any small introduction of infection into the population will eventually die out, and the system will return to its disease-free state. Epidemiologically, this result confirms that when the basic reproduction number $R_0 < 1$, the disease cannot invade or persist in the population.

2.8. Local Stability of Endemic Equilibrium Point

Theorem 2.3. The regional resilience of the persistence equilibrium of the proposed model is locally asymptotically stable if $R_0 < 1$ and unstable if otherwise.

Proof. Suppose,
$$S = a + S^*$$
, $I = b + I^*$, $Q = c + Q^*$, $R = x + R^*$, $B = y + B^*$, $H = f + H^*$.

Linearizing equation 2.1 to obtain $\frac{da}{dt} = \Lambda - \lambda ay + wx - \mu a$.

The characteristic equation obtained from its Jacobian matrix is as follows;

$$J = \begin{bmatrix} -(B\lambda + \mu) & 0 & 0 & w & -\lambda S & 0 \\ B\lambda & -(\delta + \mu + \alpha_1) & 0 & 0 & \lambda S & 0 \\ 0 & \delta & -(\varepsilon + \alpha_2 + \mu) & 0 & 0 & 0 \\ 0 & 0 & \varepsilon & -(\mu + w) & 0 & 0 \\ 0 & \eta & 0 & 0 & -(H\lambda + d + r) & -\lambda B \\ 0 & 0 & 0 & 0 & 0 & -\alpha \end{bmatrix}.$$

The resulting eigen value of the above matrix is obtained as

$$\lambda^{6} - [(p+q+s)(r+w+w) + pq + rs] + \lambda^{5}[(p+t)(q+s) + tw + rs] - [pqs(r+q) + pt(r+t)] + \lambda^{4}[qrw(p+q) + qr(p+q+s)]\lambda^{3} + [pt+ps+qs+pr]\lambda^{2} + [(t+p)(q+r)]\lambda^{1} + pqrstw = 0.$$

Therefore, the regional resilience of the Eigen values in the model invariant region of R_6^+ is asymptotically stable.

2.9. Global Stability of the Disease-Free Equilibrium

To analyses the global stability of the disease-free equilibrium (DFE) of the given cholera model, at DFE, the infected compartments (I, Q, B) = 0 i.e. the disease is absent in the population.

Setting I=0, Q=0, B=0 in the system, we solve for the equilibrium values of the remaining variables;

$$E_0 = (S^*, I^*, Q^*, R^*, B^*, H^*).$$

$$E_0 = (\frac{\Lambda}{\mu}, 0, 0, 0, 0, \frac{\rho}{\alpha}).$$

$$\begin{split} \frac{dV}{dt} = & a_1(\lambda B \frac{\Lambda}{\mu} - (\delta + \alpha_1 + \mu)I + a_2\delta I - (\xi + \alpha_2 + \mu)Q + a_3rB + \eta Q - \lambda_i H^*B - dB,) \\ \frac{dV}{dt} = & \frac{a_1\lambda B\Lambda}{\mu} - a_1(\delta + \alpha_1 + \mu)I + a_2\delta I - a_2(\xi + \alpha_2 + \mu)Q + a_3rB + a_3\eta Q - a_3\lambda_i H^*B - a_3dB, \\ \frac{dV}{dt} = & (a_1\lambda \frac{\Lambda}{\mu} + a_3r - a_3\lambda_i H^* - a_3\lambda_i H^*)B + (-a_1(\delta + \alpha_1 + \mu) + a_2\delta)I + (-a_2(\xi + \alpha_2 + \mu) + a_3\eta)Q. \end{split}$$

Choosing a_1, a_2, a_3 such that

$$a_1(\delta + \alpha_1 + \mu) > a_2\delta$$
, $a_1\lambda \frac{\Lambda}{\mu} + a_3r < a_3\lambda_i H^* - a_3d$, then $\frac{dV}{dt} \leq 0$.

Since all terms are non-positive and zero only at the DFE, this proves global asymptotically stable' Therefore, if $R_0 < 1$, then $\frac{dV}{dt} \le 0$ and E_0 is globally asymptotically stable (i.e. Cholera dies out over time, regardless of initial conditions).

2.10. Global Stability of Endemic Equilibrium

Theorem 2.4. If $S = S^*$, $I = I^*$, $Q = Q^*$, $R = R^*$, $B = B^*$ and $H = H^*$ and $Y \prec W$, with unstable R < 1, then system 2.2 is globally asymptotically stable for $R_0 > 1$.

Proof. The Lyaponuv function is used to obtain global stability utilizing the developed Lyaponuv function by [32],

$$P = (S^*, I^*, Q^*, R^*, B^*, H^*) = (S - S^* - S^* \log \frac{S}{S^*}) + (I - I^* - I^* \log \frac{I}{I^*}) + (Q - Q^* - Q^* \log \frac{Q}{Q^*}) + (R - R^* - R^* \log \frac{R}{R^*}) + (B - B^* - B^* \log \frac{B}{B^*}) + (H - H^* - H^* \log \frac{H}{H^*})$$
(2.18)

Through direct calculation, we derive the Lyaponuv function for the solution of equation 2.18 as follows;

$$\frac{dP}{dt} = \frac{dS}{dt} \left(\frac{S}{S^*} \right) \frac{dS}{dt} + \frac{dI}{dt} - \left(\frac{I}{I^*} \right) \frac{dI}{dt} + \frac{dQ}{dt} - \left(\frac{Q}{Q^*} \right) \frac{dQ}{dt} + \frac{dR}{dt} - \left(\frac{R}{R^*} \right) \frac{dR}{dt} + \frac{dB}{dt} - \left(\frac{B}{B^*} \right) \frac{dB}{dt} + \frac{dH}{dt} - \left(\frac{H}{H^*} \right) \frac{dH}{dt}$$

$$\begin{split} \frac{dP}{dt} = & \Lambda - \lambda B(t)S(t) + wR(t) - \mu S(t) - (\frac{S}{S^*})[\Lambda - \lambda B(t)S(t) + wR(t) - \mu S(t) + \lambda B(t)S(t) \\ & - (\delta + \alpha_1 + \mu)I(t) - (\frac{I}{I^*})\lambda B(t)S(t) - (\delta + \alpha_1 + \mu)I(t) + \delta I(t) - (\xi + \alpha_2 + \mu)Q(t) - (\frac{Q}{Q^*})\delta I(t) - (\xi + \alpha_2 + \mu)Q(t) + \xi Q(t) - (w + \mu)R(t) - (\frac{R}{R^*})\xi Q(t) - (w + \mu)R(t) + rB(t) + \eta I(t) - \lambda_i H(t)B(t) - dB(t) - (\frac{B}{B^*})rB(t) + \eta I(t) - \lambda_i H(t)B(t) - dB(t) + \rho - \alpha H(t) - (\frac{H}{H^*})\rho - \alpha H(t) \end{split}$$

Since the polynomial has a positive sign throughout analysis, Descartes's rule of signs is satisfied. Therefore, the polynomial cannot have any negative roots that are real numbers. After this result, applying the Routh Hurwitz condition gives another way to look at the polynomial and highlights its unique features.

$$\begin{split} \frac{dP}{dt} = & \Lambda - \lambda B(t)S(t) + wR(t) - \mu S(t) - (\frac{S}{S^*})\Lambda + (\frac{S}{S^*})[\lambda B(t)S(t) - wR(t) + \mu S(t)] + \lambda B(t)S(t) \\ & - (\delta + \alpha_1 + \mu)I(t) - (\frac{I}{I^*})\lambda B(t)S(t) + (\frac{I}{I^*})(\delta + \alpha_1 + \mu)I(t) + \delta I(t) - (\xi + \alpha_2 + \mu)Q(t) - (\frac{Q}{Q^*})\delta I(t) + (\frac{Q}{Q^*})(\xi + \alpha_2 + \mu)Q(t) + \xi Q(t) - (w + \mu)R(t) - (\frac{R}{R^*})\xi Q(t) + (\frac{R}{R^*})(w + \mu) \\ & R(t) + rB(t) + \eta I(t) - \lambda_i H(t)B(t) - dB(t) - (\frac{B}{B^*})rB(t) + \eta I(t) + (\frac{B}{B^*})\lambda_i H(t)B(t) - dB(t) + \rho - \alpha H(t) - (\frac{H}{H^*})\rho + (\frac{H}{H^*})\alpha H(t) \end{split}$$

By rearranging terms i.e both positive and negative terms we have,

$$\frac{dP}{dt} = Y - W$$

$$Y = \Lambda - \lambda B(t)S(t) + wR(t) - \mu S(t) + (\frac{S}{S^*})[\lambda B(t)S(t) - wR(t) + \mu S(t)] + \lambda B(t)S(t)$$

$$- (\delta + \alpha_1 + \mu)I(t) + (\frac{I}{I^*})(\delta + \alpha_1 + \mu)I(t) + \delta I(t) - (\xi + \alpha_2 + \mu)Q(t) + (\frac{Q}{Q^*})(\xi + \alpha_2 + \mu)Q(t) + \xi Q(t) - (w + \mu)R(t) + (\frac{R}{R^*})(w + \mu)R(t) + rB(t) + \eta I(t) - \lambda_i H(t)B(t) - dB(t) + (\frac{B}{R^*})\lambda_i H(t)B(t) - dB(t) + \rho - \alpha H(t) + (\frac{H}{H^*})\alpha H(t)$$

And

$$W = (\frac{S}{S^*})\Lambda - (\frac{I}{I^*})\lambda B(t)S(t) - (\frac{Q}{Q^*})\delta I(t) - (\frac{R}{R^*})\xi Q(t) - (\frac{B}{B^*})rB(t) + \eta I(t) - (\frac{H}{H^*})\rho I(t) - (\frac{R}{H^*})\rho I(t) - (\frac{R}{H^*})\rho$$

Hence, if Y < W, then $\frac{dP}{dt} = 0$ if and only if

$$S = S^*, I = I^*, Q = Q^*, R = R^*, B = B^*$$
and $H = H^*.$

Thus, we have the largest compartment invariant set to be equal to $\left\{(S^*,I^*,Q^*,R^*,B^*,H^*)\in\Gamma,\frac{dP}{dt}=0\right\}$ where E^* is a singleton of the endemic equilibrium. For this reason, the Lasalle's invariant approach shows that Γ if Y< W, the E^* is globally asymptotically stable.

3. Numerical Simulation

To illustrate the qualitative behavior of the proposed model and validate the analytical results, numerical simulations were carried out using parameter values obtained from the literature and reasonable assumptions where data were unavailable.

3.1. Application of Laplace-Adomian Decomposition Method (LADM)

Using LADM, the equation is solved and the solution, an analytical series, is found by decomposing difficult non-linear functions into easy-to-calculate Adomian polynomials. Hence, LADM uses the formula to solve below equations.

With initial conditions;

$$S(0) = S_0, I(0) = I_0, Q(0) = Q_0, R(0) = R_0, B(0) = B_0, H(0) = H_0$$

$$L\left\{{}^C F^Z S(t)\right\} = L\left\{\Lambda - \lambda B(t) S(t) + w R(t) - \mu S(t)\right\},$$

$$L\left\{{}^C F^Z I(t)\right\} = L\left\{\lambda B(t) S(t) - (\delta + \alpha_1 + \mu) I(t)\right\},$$

$$L\left\{{}^C F^Z Q(t)\right\} = L\left\{\delta I(t) - (\xi + \alpha_2 + \mu) Q(t)\right\},$$

$$L\left\{{}^C F^Z R(t)\right\} = L\left\{\xi Q(t) - (w + \mu) R(t)\right\},$$

$$L\left\{{}^C F^Z B(t)\right\} = L\left\{r B(t) + \eta I(t) - \lambda_i H(t) B(t) - d B(t)\right\},$$

$$L\left\{{}^C F^Z H(t)\right\} = L\left\{\rho - \alpha H(t)\right\}.$$

Let S, I, Q, R, B and H be infinite series such that;

$$S = \sum_{i=0}^{z} S_i, I = \sum_{i=0}^{z} I_i, Q = \sum_{i=0}^{z} Q_i, R = \sum_{i=0}^{z} R_i, B = \sum_{i=0}^{z} B_i, H = \sum_{i=0}^{z} H_i$$

BS and HB are non-linear term of the model and it can be broken down by Adomian. Let

$$BS = \sum_{i=0}^{z} M_i$$
 and $HB = \sum_{i=0}^{z} N_i$

Where M_i and N_i are Adomian polynomial such that:

$$M_{i} = \frac{1}{\Gamma(i+1)} \frac{d^{i}}{d\lambda^{i}} \left[\sum_{\alpha=0}^{\infty} \lambda^{x} B_{x} \sum_{\alpha=0}^{\infty} \lambda^{x} S_{x} \right]_{\lambda=0} \quad \text{and} \quad N_{i} = \frac{1}{\Gamma(i+1)} \frac{d^{i}}{d\lambda^{i}} \left[\sum_{\alpha=0}^{\infty} \lambda^{x} H_{x} \sum_{\alpha=0}^{\infty} \lambda^{x} B_{x} \right]_{\lambda=0}$$

Taking,

$$S_{0} = v_{1}, I_{0} = v_{2}, Q_{0} = v_{3}, R_{0} = v_{4}, B_{0} = v_{5}, H_{0} = v_{6}$$

$$S_{1}(t) = t^{z}(\Lambda - v_{1}(\lambda v_{5} + \mu) + v_{4}w) \frac{1}{\Gamma(1+z)}$$

$$I_{1}(t) = t^{z}(\lambda v_{1}v_{5} - (\delta + \alpha_{1} + \mu)v_{2}) \frac{1}{\Gamma(1+z)}$$

$$Q_{1}(t) = t^{z}(v_{2}\delta - v_{3}(\varepsilon + \alpha_{2} + \mu)) \frac{1}{\Gamma(1+z)}$$

$$R_{1}(t) = t^{z}(v_{3}\varepsilon - v_{4}(w + \mu)) \frac{1}{\Gamma(1+z)}$$

$$B_{1}(t) = t^{z}(v_{5}(r - \lambda_{i}v_{6} - d) + \eta v_{2}) \frac{1}{\Gamma(1+z)}$$

$$H_{1}(t) = t^{z}(\rho - \alpha v_{6}) \frac{1}{\Gamma(1+z)}$$

$$S_{2}(t) = \left\{ \Lambda - \lambda(v_{5}[(\Lambda - v_{1}(\lambda v_{5} + \mu) + wv_{4}] \frac{t^{2z}}{\Gamma(1+2z)} + v_{1}[v_{5}(r - \lambda_{i}v_{6} - d) + \eta v_{2}] \right\}$$

$$\frac{t^{2z}}{\Gamma(1+2z)} + w\left[v_{3}\varepsilon - v_{4}(w + \mu)\right] \frac{t^{2z}}{\Gamma(1+2z)} - \mu\left[\Lambda - v_{1}(\lambda v_{5} + \mu) + v_{4}w\right] \frac{t^{2z}}{\Gamma(1+2z)}$$

$$I_{2}(t) = \lambda v_{5} \left[(\Lambda - v_{1}(\lambda v_{5} + \mu) + v_{4}w) \right] \frac{t^{2z}}{\Gamma(1+2z)} + v_{1}[v_{5}(r - \lambda_{i}v_{6} - d) + \eta v_{2}] \frac{t^{2z}}{\Gamma(1+2z)} - (\delta + \alpha_{1} + \mu)\lambda v_{1}v_{5} - (\delta + \alpha_{1} + \mu)v_{2} \frac{t^{2z}}{\Gamma(1+2z)}$$

$$Q_{2}(t) = \delta(\lambda v_{1}v_{5} - (\delta + \alpha_{1} + \mu)v_{2}) \frac{t^{2z}}{\Gamma(1+2z)} - (\varepsilon + \alpha_{2} + \mu)[v_{2}\delta - v_{3}(\varepsilon + \alpha_{2} + \mu)) \frac{t^{2z}}{\Gamma(1+2z)}$$
$$R_{2}(t) = \varepsilon[v_{2}\delta - v_{3}(\varepsilon + \alpha_{2} + \mu)) \frac{t^{2z}}{\Gamma(1+2z)} - (w + \mu)[v_{3}\varepsilon - v_{4}(w + \mu)) \frac{t^{2z}}{\Gamma(1+2z)}$$

$$B_{2}(t) = \left\{ r(t^{z}[v_{5}(r - \lambda_{i}v_{6} - d) + \eta v_{2}] \frac{t^{2z}}{\Gamma(1 + 2z)} + \eta t^{z}[\lambda v_{1}v_{5} - (\delta + \alpha_{1} + \mu)v_{2}] \frac{t^{2z}}{\Gamma(1 + 2z)} - \lambda_{i}\{v_{6}t^{z}\} \right\}$$

$$[v_{5}(r - \lambda_{i}v_{6} - d) + \eta v_{2}] \frac{t^{2z}}{\Gamma(1 + 2z)} + t^{z}v_{5}(\rho - \alpha v_{6}) \frac{t^{2z}}{\Gamma(1 + 2z)} \right\} - dt^{z}[v_{5}(r - \lambda_{i}v_{6} - d) + \eta v_{2}]$$

$$\frac{t^{2z}}{\Gamma(1 + 2z)}$$

$$H_2(t) = (\rho - \alpha)(\rho - \alpha v_6) \frac{t^{2z}}{\Gamma(1 + 2z)}$$
$$t^z (\Lambda - v_1(\lambda v_5 + \mu) + v_4 w) \frac{1}{\Gamma(1 + z)}$$

Table 3.2: Parameter values and initial conditions

Parameter	Description	Value
Λ	Recruitment rate	$24.4N(0)/365000 (day^{-1})$
μ	Natural death rate	$2.2493 \times 10^{-5} (day^{-1})$
λ	Force of infection	$0.8 (day^{-1})$
r	Multiplication rate of bacteria via binary fission	4.158 (day ⁻¹)
ω	Immunity waning rate	$0.4/365 (day^{-1})$
δ	Quarantine rate	$0.05 (day^{-1})$
γ	Recovery rate	$0.2 (day^{-1})$
α_1	Death rate (infected)	$0.015 (day^{-1})$
α_2	Death rate (quarantined)	$0.0001 (day^{-1})$
η	Shedding rate (infected)	$10 \text{ (cell/mday}^{-1} \text{person}^{-1})$
λ_1	Clearance rate of pathogens due to hy-	$0.3, 0 \le \lambda_1 \le 1,$
	gienic measure	
ρ	Investment (Effort) rate to increase hygiene levels.	0.5
Λ	the natural decay of hygiene measures	$0.3, 0 \le \lambda_1 \le 1,$
	(e.g., infrastructure decay or reduced	
	public	
d	Bacteria death rate	$0.33 (day^{-1})$
S(0)	Susceptible individuals at $t = 0$	570 (person)
I(0)	Infected individuals at $t = 0$	170 (person)
Q(0)	Quarantined individuals at $t = 0$	0 (person)
R(0)	Recovered individuals at $t = 0$	0 (person)
B(0)	Bacterial concentration at $t = 0$	$275 \times 10^3 \text{ (cell/ml)}$

Table 3.2 above summarizes the parameter values and initial conditions used in the SIQRB model. These include key rates such as transmission, recovery, quarantine, and bacterial growth, along with the initial population values for S(0), I(0), Q(0), R(0), and B(0). The table provides the baseline setup necessary for simulating the cholera transmission dynamics.

3.2. Simulation Result

Utilizing the results obtained from LADM with Caputo derivatives on equation 2.2 and parameter values in Table 3.2, we perform numerical simulations to observe how the system acts in various situations. They study in detail how immunity problems following treatment and interventions to raise hygiene affect the way diseases are passed on. The study looks at how these factors cause changes in the number of susceptible, infected and pathogen individuals so that its role in the disease spread can be better understood. The analysis gives understanding of the link between hygiene control and the number of people experiencing relapses, indicating possible steps to reduce infections and improve handling of diseases.

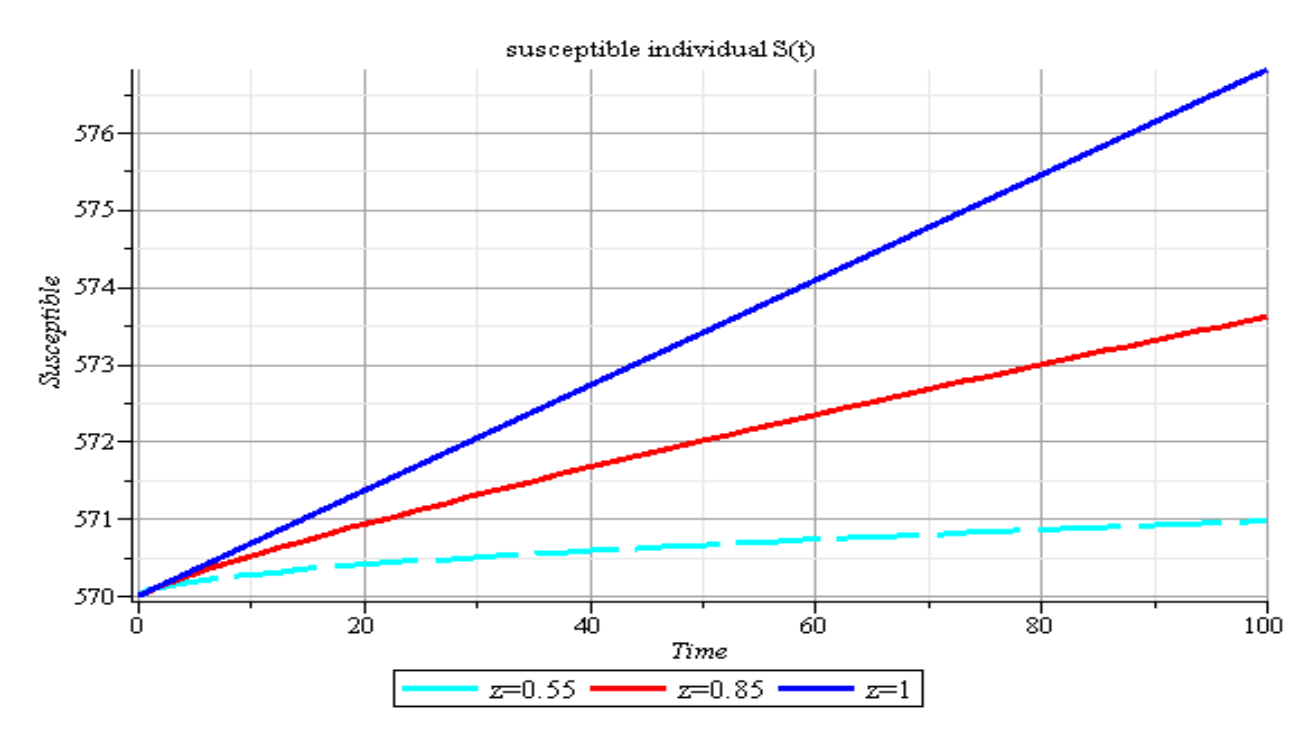


Figure 3.2: Plot shows the behavior of S(t) at different values of fractional order z

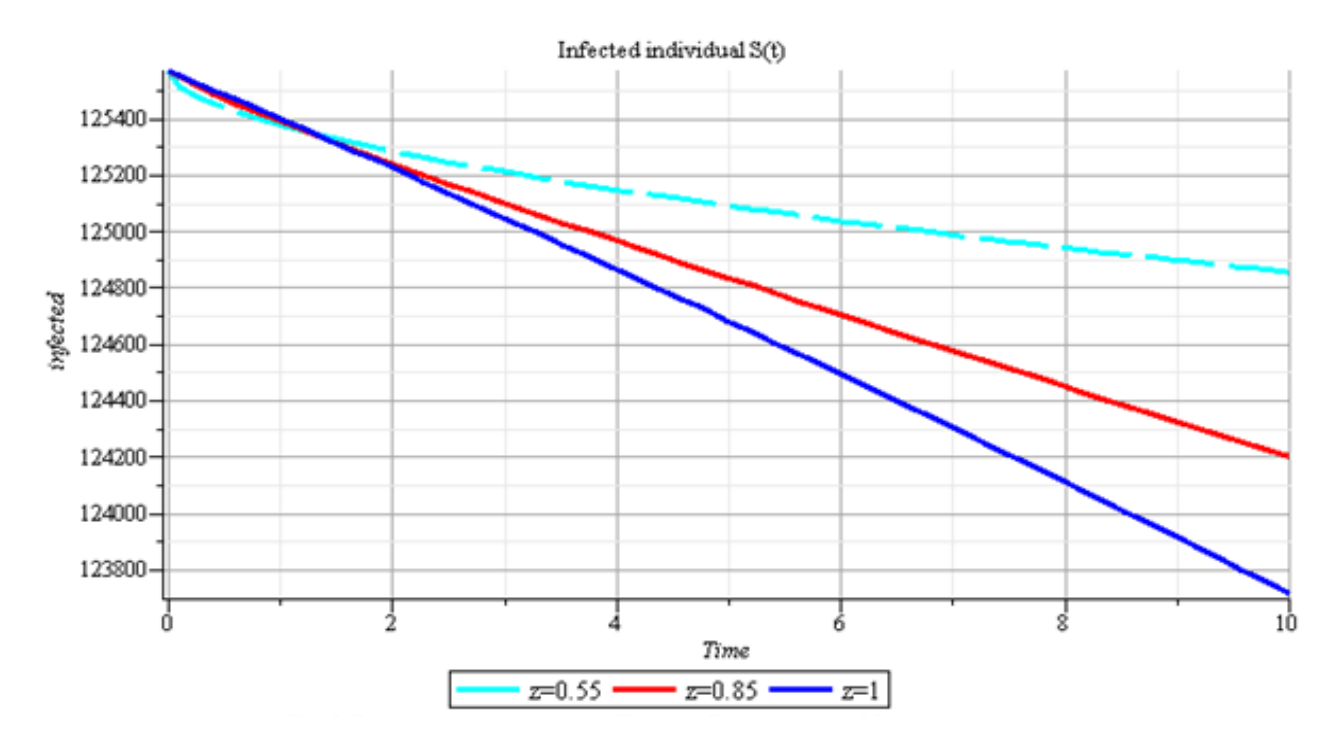


Figure 3.3: Plot shows the behavior of I(t) at different values of fractional order z

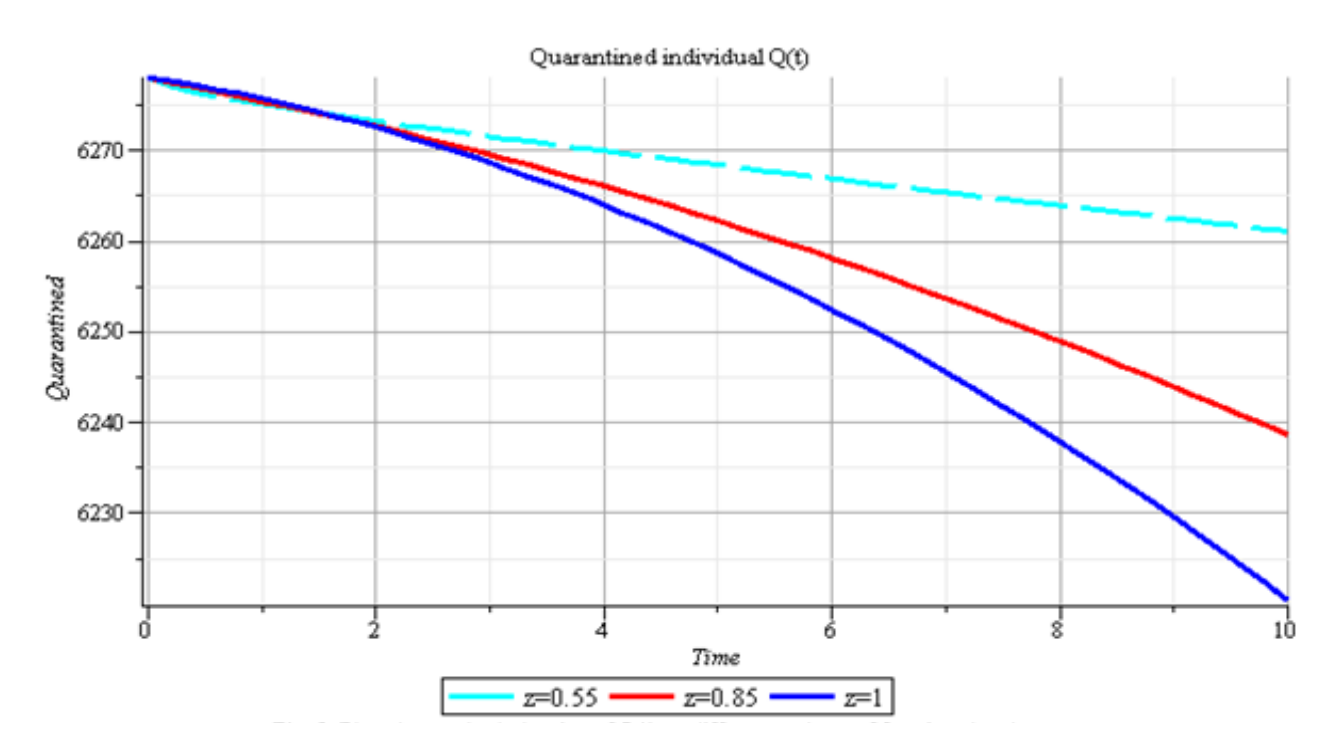


Figure 3.4: Plot shows the behavior of Q(t) at different values of fractional order z

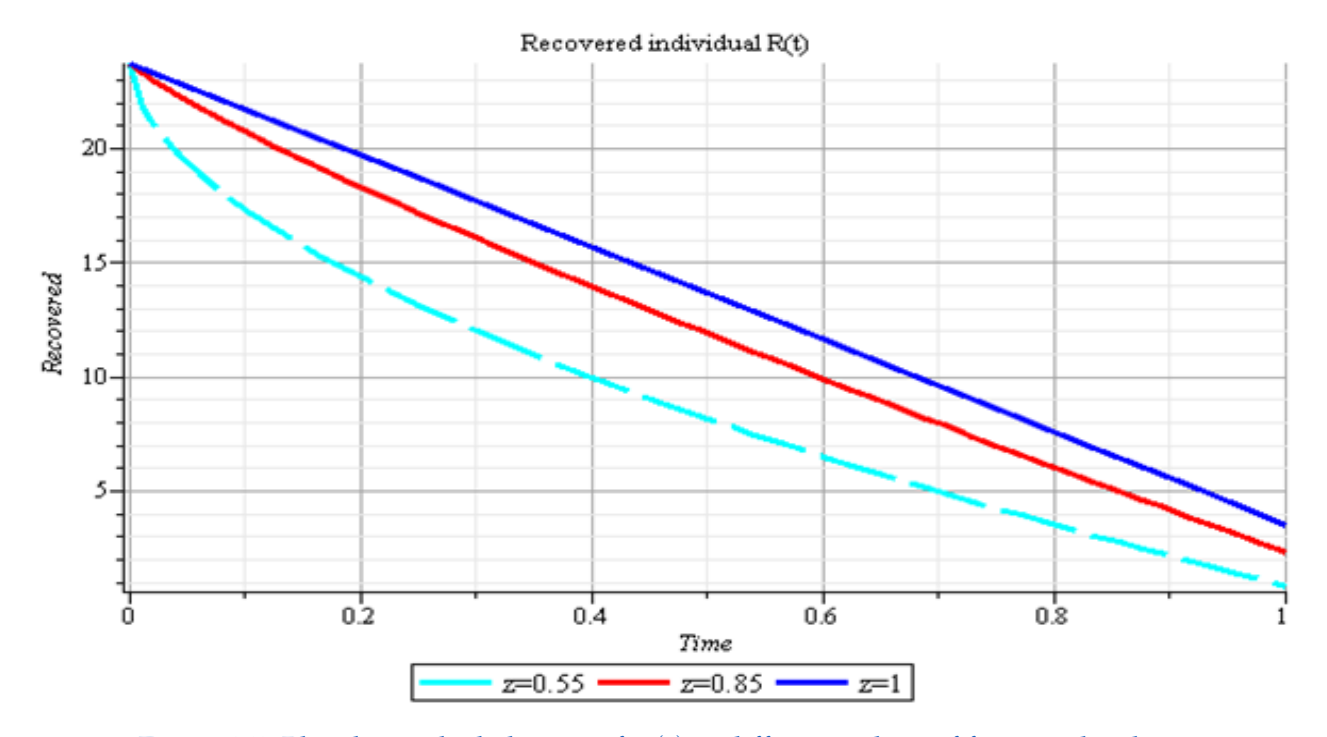


Figure 3.5: Plot shows the behavior of R(t) at different values of fractional order z

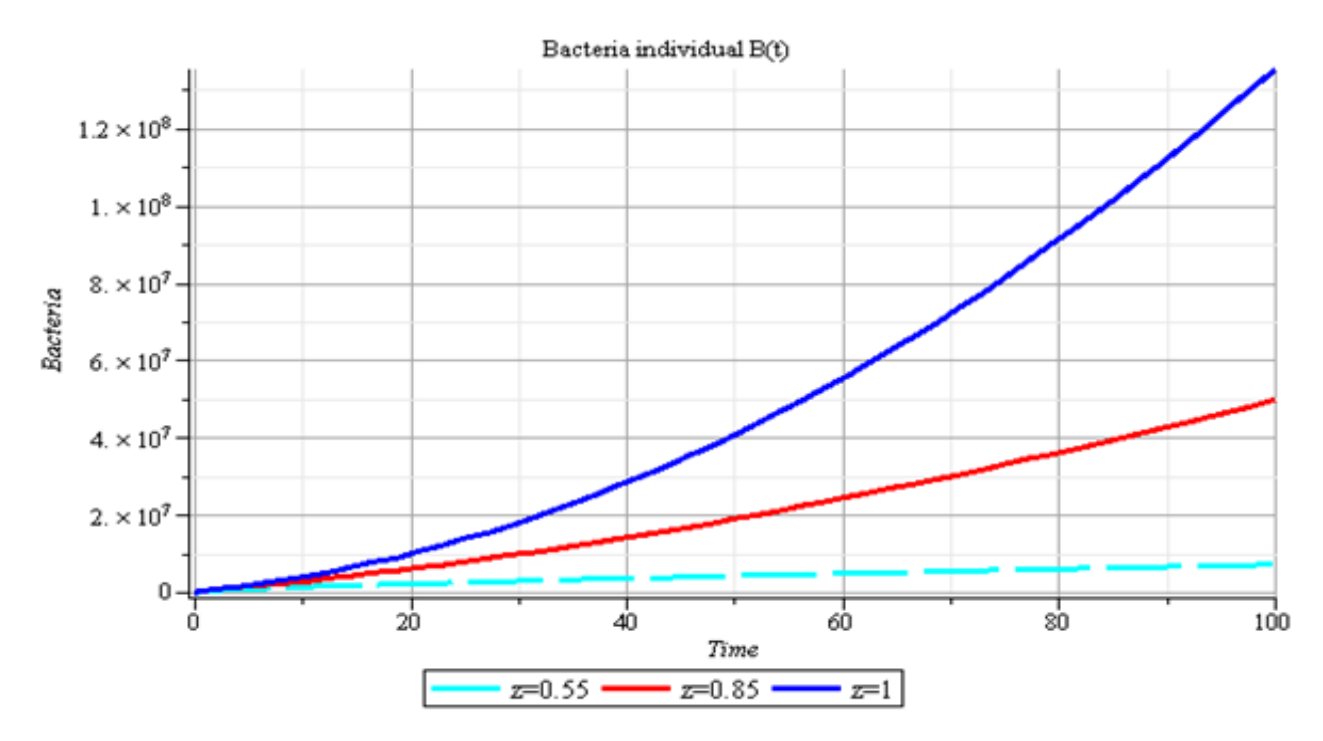


Figure 3.6: Plot shows the behavior of B(t) at different values of fractional order z

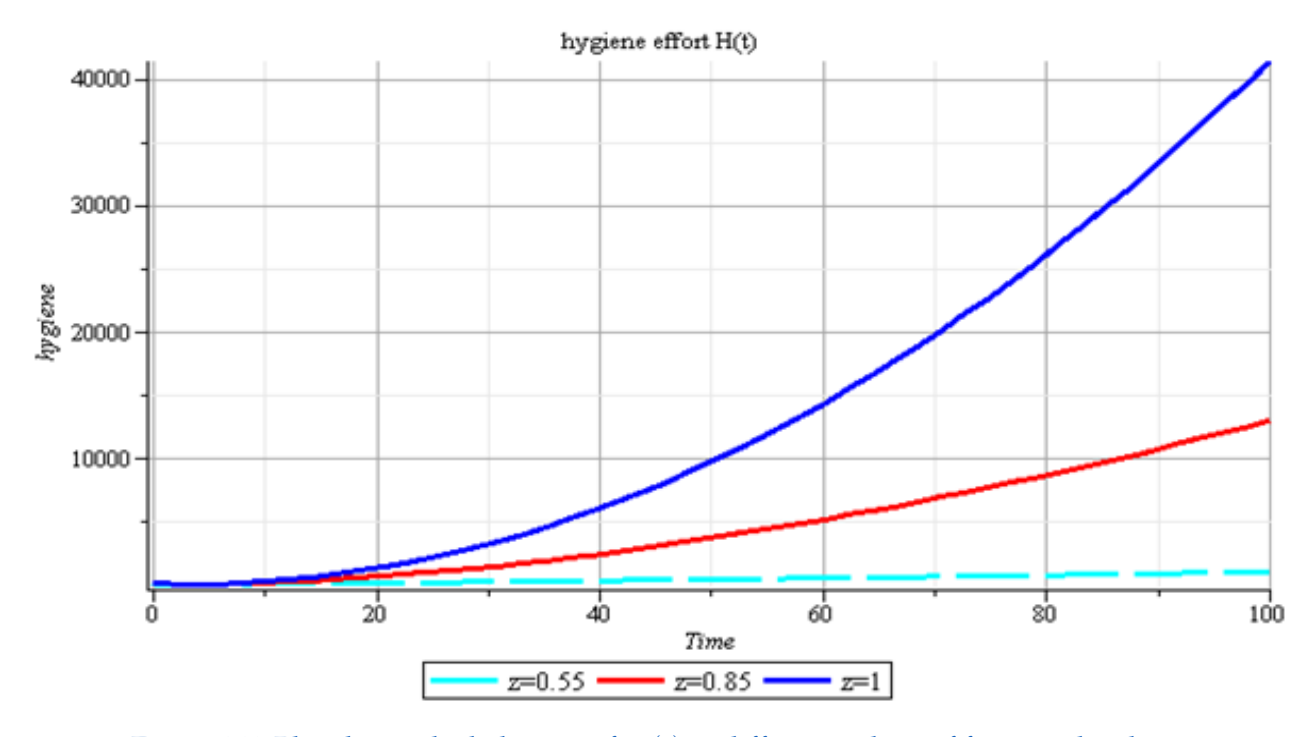


Figure 3.7: Plot shows the behavior of H(t) at different values of fractional order z

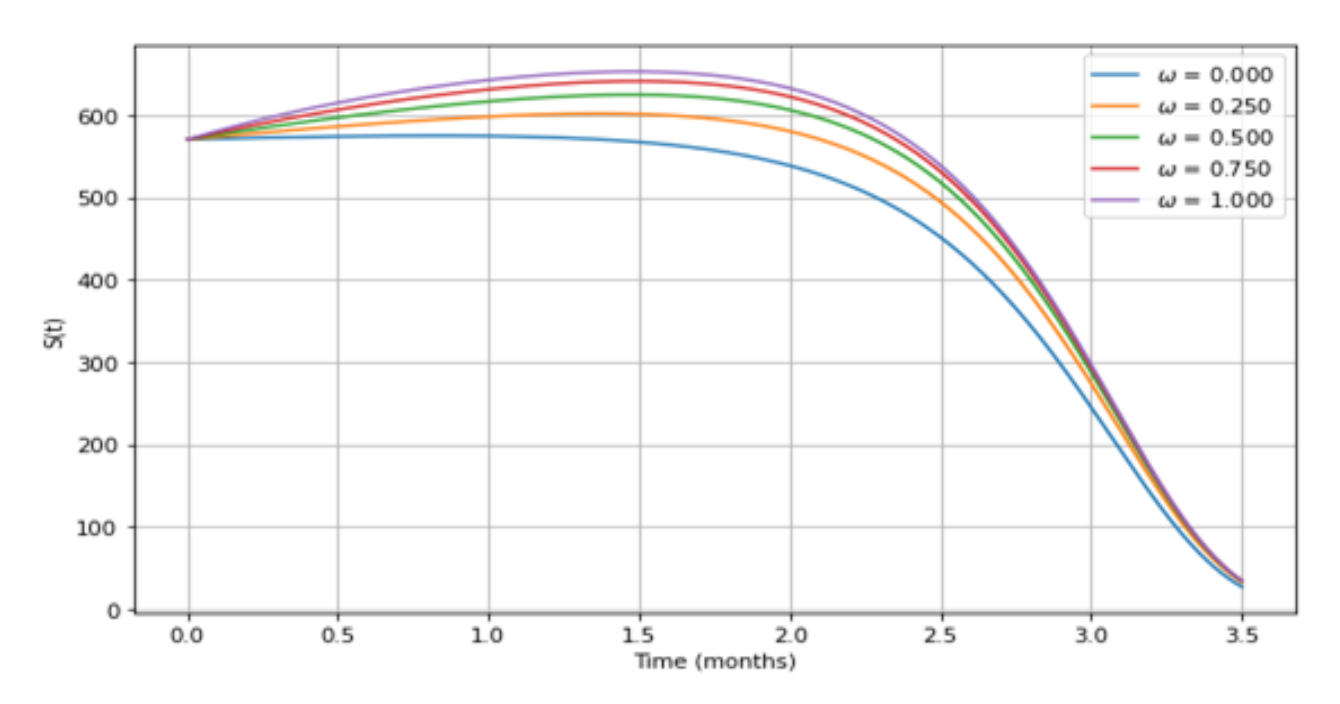


Figure 3.8: Effect of Relapse rate of recovered individuals post immunity gained from treatment on S(t)

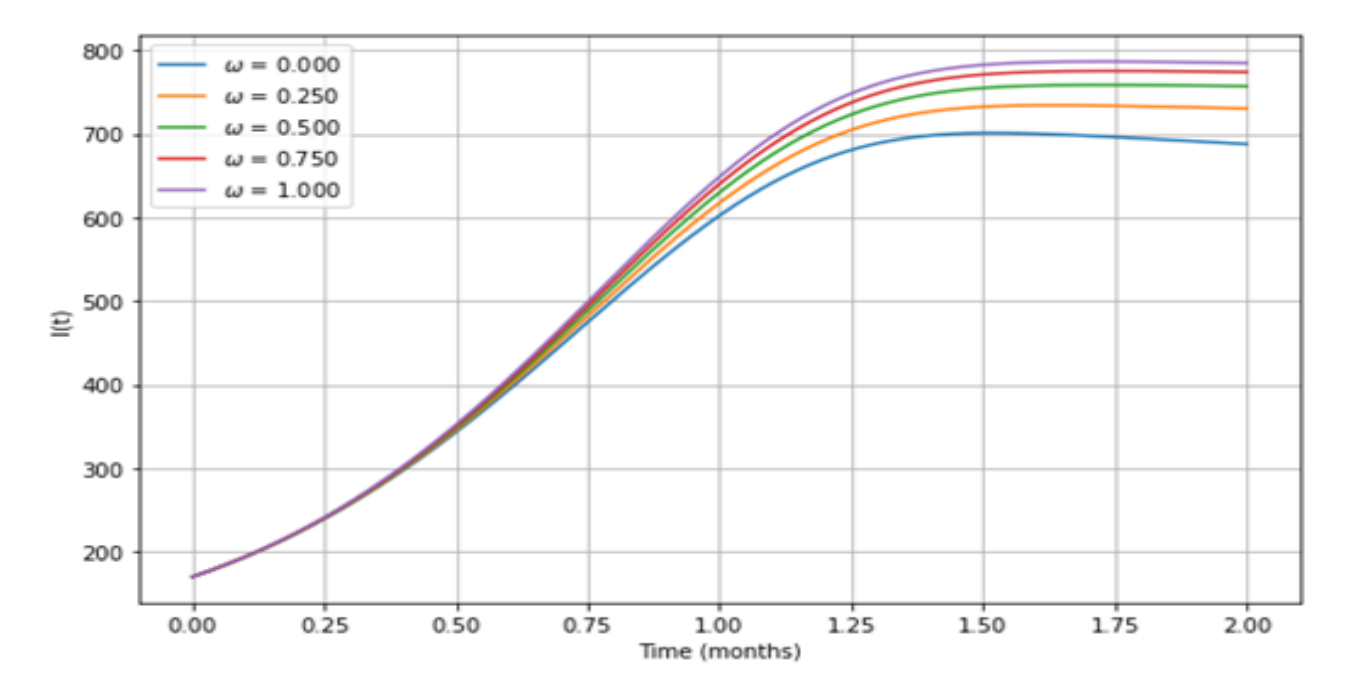


Figure 3.9: Effect of Relapse rate of recovered individuals post immunity gained from treatment on I(t)

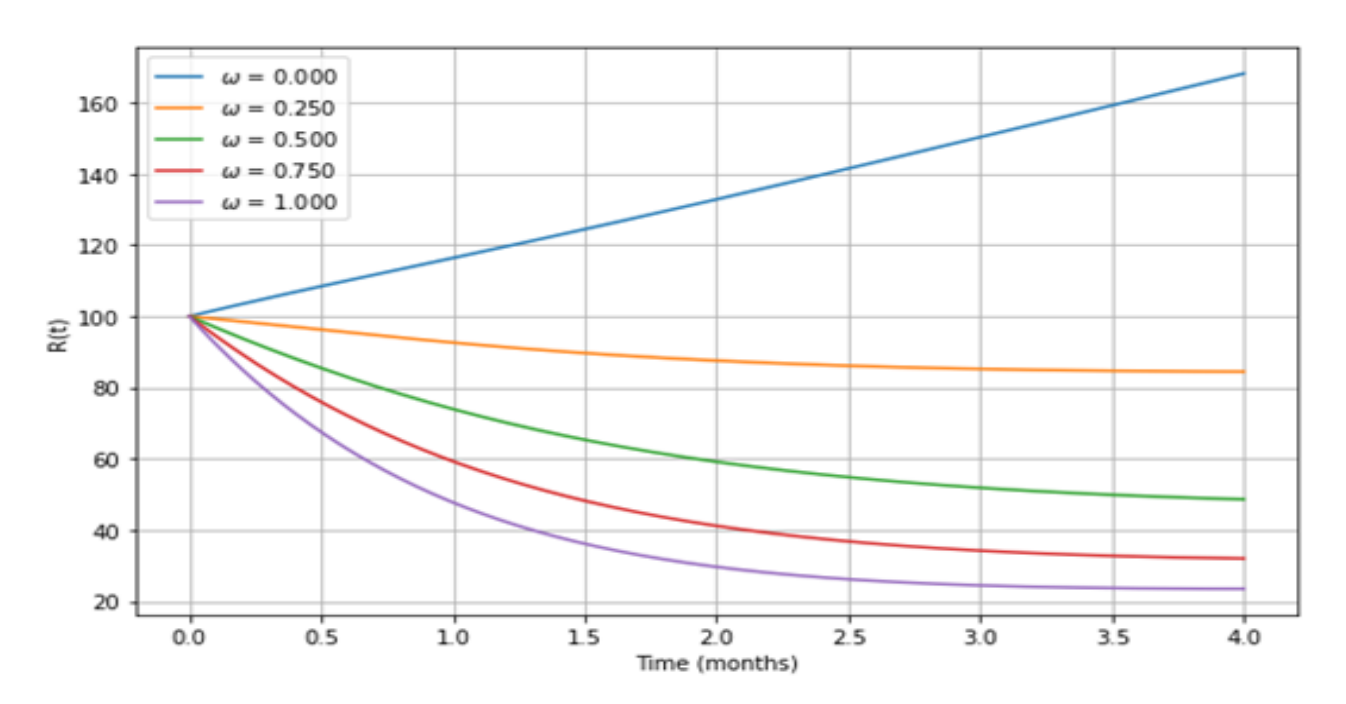


Figure 3.10: Effect of Relapse rate of recovered individuals post immunity gained from treatment on I(t)

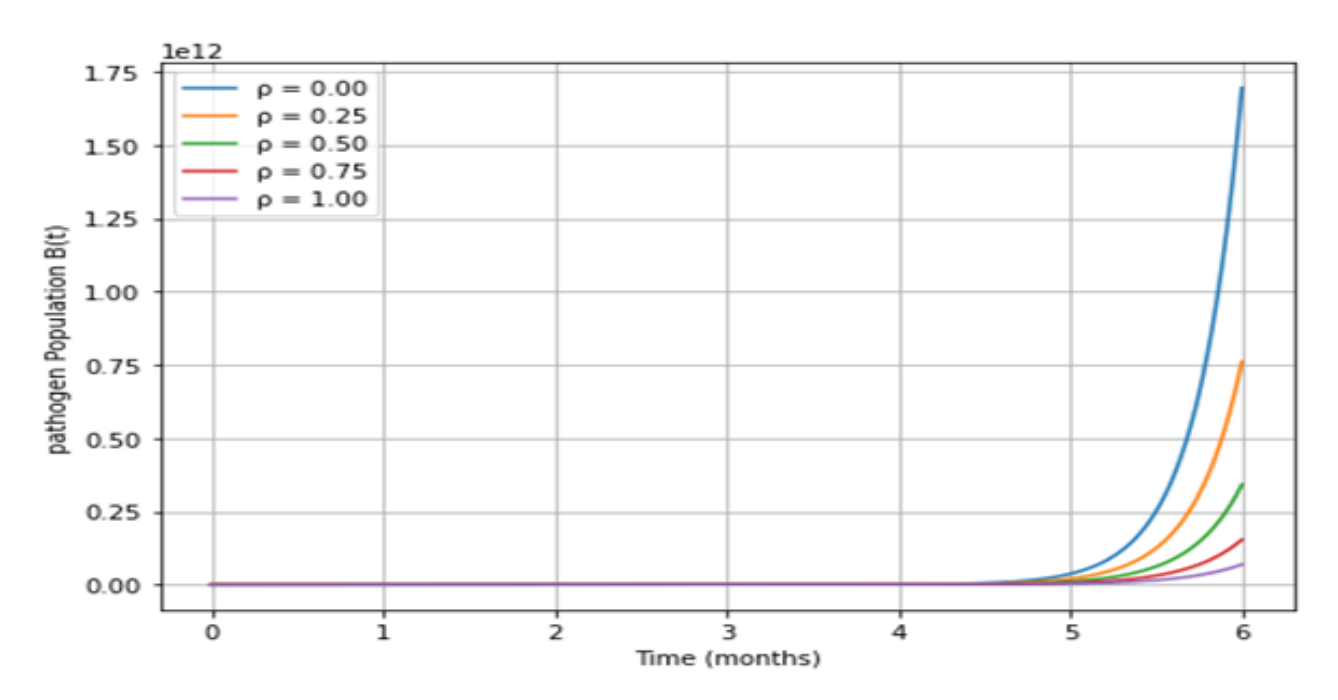


Figure 3.11: Effect of effort rate to increase hygienic level on pathogen population

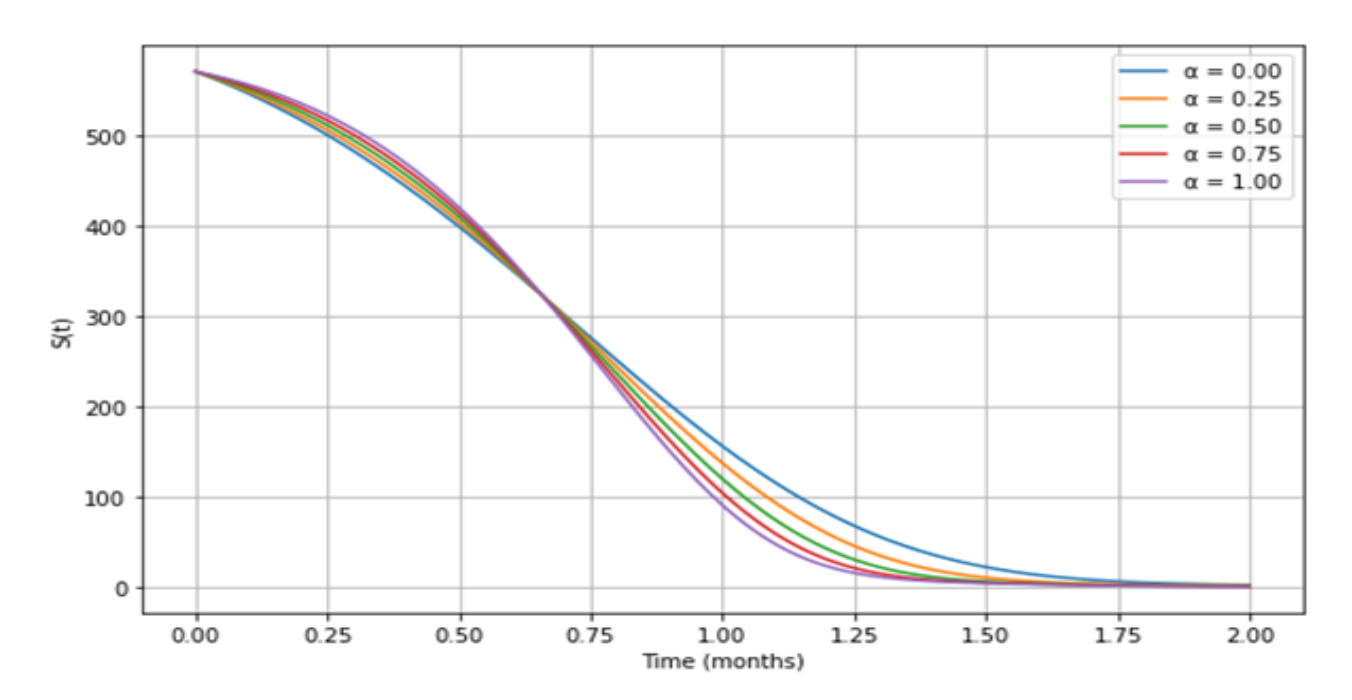


Figure 3.12: Impact of decay rate of hygienic efforts on Susceptible population

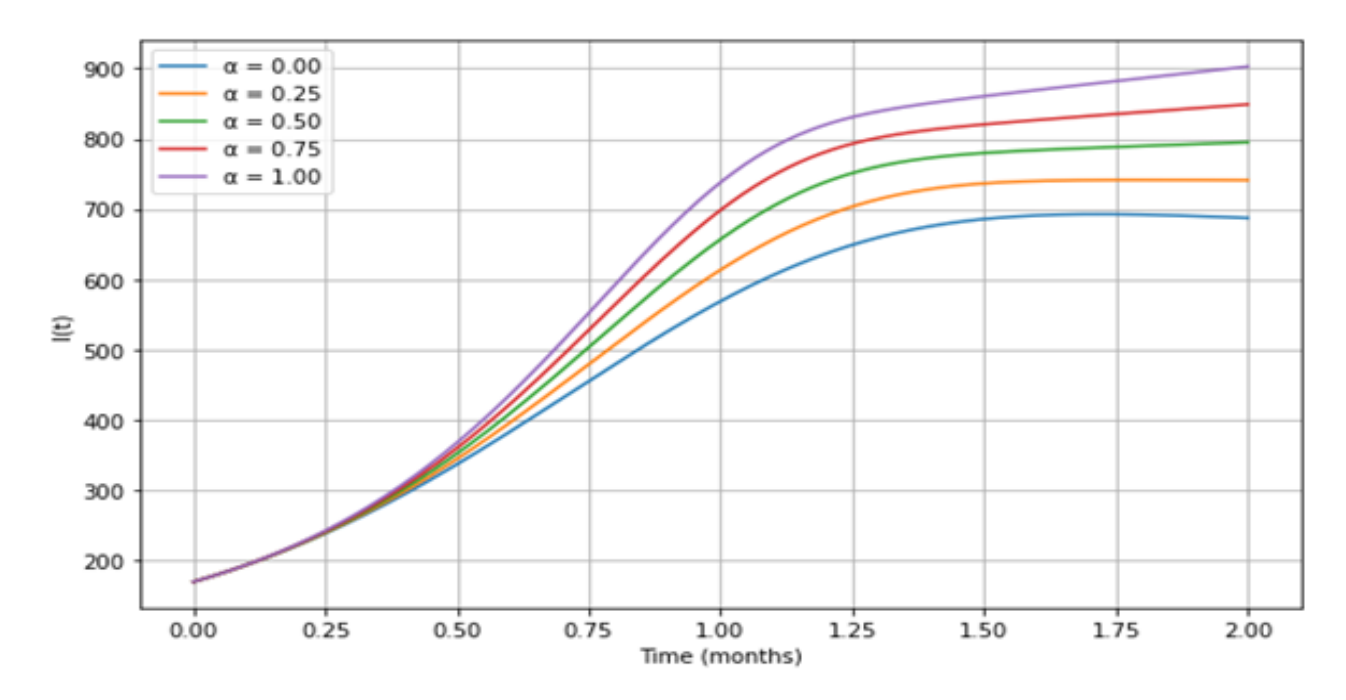


Figure 3.13: Impact of decay rate of hygienic efforts on Infected population

Explanation and Interpretations of Results

Figure 3.2: The Behaviour of S(t) (Susceptible Individuals) at Different Values of Fractional Order z

Figure 3.2 illustrates how the susceptible population S(t) responds to varying fractional-order values z. As z decreases from 1 toward lower fractional values, the decline of S(t) becomes slower, reflecting the memory effect introduced by the fractional-order derivative. This suggests that fractional dynamics prolong the time individuals remain susceptible, thereby delaying the onset of infection in the population. The figure demonstrates that fractional models capture more realistic disease progression by accounting for population heterogeneity and historical dependence.

Figure 3.3: The Behaviour of I(t) (Infected Individuals) at Different Fractional Orders z

Figure 3.3 illustrates the time evolution of the infected population I(t) for three different values of the fractional order z=0.55, 0.85, and 1. The plot shows a monotonic decrease in the number of Infected individuals over time across all fractional orders, indicating that the infection tends toward eradication in the long run. Notably, the rate of decline becomes steeper as z increases, with the classical case (z=1) exhibiting the fastest reduction in infection levels. This result suggests that higher fractional orders accelerate the convergence of the system toward the disease-free equilibrium, implying a more effective disease elimination process under classical (integer-order) dynamics compared to fractional-order dynamics with z<1.

Figure 3.4 : Behaviour of Q(t) (Quarantined Individuals) at Different Fractional Orders z

Figure 3.4 depicts the dynamics of the quarantined population Q(t) for the same fractional orders. Similar to the infected compartment, the number of quarantined individuals gradually declines with time, reflecting the successful removal of infected individuals from isolation as they either recover or exit the system. The plot also shows that for higher fractional orders, the decrease in quarantined individuals is faster. The curve for z=1 drops more sharply than that of z=0.55, indicating that memory effects (captured by fractional orders less than one) tend to slow down the rate at which quarantined individuals leave the compartment.

Figure 3.5: Behavior of R(t) (Recovered Individuals) at Different Fractional Orders z

Figure 3.5 presents the time evolution of the recovered population R(t). In contrast to the infected and quarantined compartments, R(t) shows a steady increase over time, indicating continuous recovery from infection. The curves reveal that higher fractional orders result in a more rapid growth of recovered individuals, with the classical model (z=1) producing the highest recovery rates. For z=0.55, the recovery curve rises more slowly, highlighting the impact of fractional-order dynamics in delaying the buildup of immunity within the population.

Figure 3.6 The Behaviour of B(t) at Different Values of Fractional Order z

Here, B(t) represents the concentration of pathogens in the environment. The figure shows that lower fractional orders delay the peak of pathogen concentration, leading to a more persistent but less intense environmental contamination profile. This aligns with the interpretation that memory effects slow the system's dynamics, resulting in more extended but less explosive outbreaks.

Figure 3.7 The Behaviour of H(t) at Different Values of Fractional Order z

For the hygiene-related compartment H(t), fractional-order effects produce a slower adjustment toward equilibrium. Lower z-values indicate that changes in hygiene effort take longer to influence the system, leading to delayed reductions in transmission risk. This figure reinforces the notion that fractional models better capture gradual behavioural adaptation over time.

Figure 3.8 Effect of Relapse Rate of Recovered Individuals on S(t)

An increase in the relapse rate leads to a rise in the susceptible population S(t), as individuals lose immunity and return to the pool of susceptible. This demonstrates that relapse acts as a replenishing mechanism for the susceptible class, potentially sustaining transmission. Lower relapse rates keep S(t) at minimal levels, which is favourable for disease elimination.

Figure 3.9 Effect of Relapse Rate of Recovered Individuals on I(t)

As relapse rate increases, I(t) grows significantly, showing that frequent relapses fuel continued transmission and increase the infection burden. This underscores the importance of post-treatment interventions such as follow-up monitoring or booster doses to prevent recurrent infections.

Figure 3.10 Effect of Relapse Rate of Recovered Individuals on I(t)

Figure 3.10 may explore a different parameter range or longer time horizon compared to Figure 3.9. It shows that I(t) not only increase with relapse rate but may eventually stabilize at an endemic level, indicating that relapse can sustain infection even in the absence of new external introductions. This has significant implications for long-term control strategies.

Figure 3.11 Effect of Effort Rate to Increase Hygienic Level on Pathogen Population

The figure shows a clear negative relationship between hygiene effort and pathogen population. As hygiene effort intensifies, pathogen levels drop sharply, confirming that sanitation campaigns and public health interventions effectively limit environmental transmission.

Figure 3.12 Impact of Decay Rate of Hygienic Efforts on Susceptible Population

A higher decay rate of hygiene efforts leads to an increase in S(t), reflecting that when hygiene practices wane, more individuals become susceptible due to renewed exposure. This highlights the need for sustained hygiene promotion programs to prevent resurgence of infection.

Figure 3.13 Impact of Decay Rate of Hygienic Efforts on Infected Population

Similarly, a higher decay rate increases I(t), showing that lapses in hygiene maintenance can quickly elevate disease prevalence. The figure emphasizes that infection control gains are fragile and require continuous community engagement and infrastructure maintenance.

4. Discussion

Discussion of Results

The numerical simulations provide valuable insights into how fractional-order dynamics and public health interventions influence disease transmission. As illustrated in Figure 3.2, higher fractional orders predict a faster decline in the susceptible population, indicating more extensive exposure to infection. Conversely, lower fractional orders slow this decline, reflecting stronger memory effects that delay infection spread. In Figure 3.3, this same effect leads to a slower increase in the infected population, effectively flattening the epidemic curve and suggesting that fractional-order models capture a more gradual and realistic outbreak progression. Figure 3.4 demonstrates that the size of the quarantined population is highly sensitive to the value of z. When z is closer to one, quarantine peaks earlier and higher, whereas lower values spread the quarantined burden over a longer period. This finding underscores the role of memory effects in designing intervention strategies, as they affect when and how many individuals are isolated. Similarly, Figure 3.5 reveals that recovery is delayed at lower z-values, leading to slower accumulation of immunity within the population and extending the overall epidemic duration. Environmental and behavioral dynamics are highlighted in Figure 3.6 and Figure 3.7. Figure 3.6 shows that higher z-values reduce environmental pathogen concentration, lowering the risk of bacterial overgrowth and subsequent exposure. Figure

3.7 demonstrates that memory effects strengthen the persistence of hygiene practices, helping communities sustain protective behaviors over time. Figure 3.8 to Figure 3.10 explore the effect of relapse rates among recovered individuals. As relapse rates increase, the number of susceptibles rises Figure 3.8, which fuels a corresponding increase in infection levels Figure 3.9 and Figure 3.10. These results emphasize the importance of ensuring long-lasting immunity after treatment to prevent reinfections and secondary outbreaks. Finally, Figure 3.11 to Figure 3.13 focus on hygiene interventions. Figure 3.11 clearly shows that increasing hygiene efforts effectively reduces pathogen population in the environment, confirming that sanitation plays a crucial role in disease control. However, Figure 3.12 and Figure 3.13 reveal that when hygienic practices decay rapidly, both susceptibility and infection prevalence rise, potentially reversing previous gains. This highlights the necessity for sustained hygiene promotion campaigns and community engagement to maintain long-term benefits. Overall, the simulations collectively demonstrate that fractional-order models capture the memory-dependent nature of disease transmission, relapse, and intervention effects more realistically than classical models. They also reaffirm the critical role of continuous hygiene efforts and robust post-treatment immunity in preventing recurrent epidemics and reducing the long-term disease burden.

5. Conclusion

This study develops a fractional-order model for cholera transmission that integrates immunity relapse, hygiene behavior, and environmental factors. Using the modified Caputo derivative and solving with the Laplace–Adomian Decomposition Method (LADM), the model captures memory effects and produces biologically valid solutions. The derived basic reproduction number and stability analysis provide a strong theoretical foundation, while numerical simulations confirm the model's ability to reflect real cholera dynamics. Findings show that waning immunity and poor hygiene extend disease persistence and increase relapse frequency, emphasizing the need for strategies that strengthen immunity and promote hygiene. This approach can be adapted to other infectious diseases, offering a valuable tool for long-term control and epidemiological forecasting.

References

- [1] D. A. Montero, R. M. Vidal, J. Velasco, S. George, Y. Lucero, L. A. Gómez, and M. O'Ryan, "Vibrio cholerae, classification, pathogenesis, immune response, and trends in vaccine development," *Frontiers in Medicine*, vol. 10, p. 1155751, 2023. View online.
- [2] B. Sit, B. Fakoya, and M. K. Waldor, "Emerging concepts in cholera vaccine design," *Annual Review of Microbiology*, vol. 76, no. 1, pp. 681–702, 2022. View online.
- [3] S. Malik, "Numerical performance of the fractional direct spreading cholera disease model: An artificial neural network approach," *Fractal & Fractional*, vol. 8, no. 7, 2024. View online.
- [4] M. F. Alharbi, "Neural network procedures for the cholera disease system with public health mediations," *Computers in Biology and Medicine*, vol. 184, p. 109471, 2025. View online.
- [5] N. Anwar, A. Fatima, M. A. Z. Raja, I. Ahmad, M. Shoaib, and A. K. Kiani, "Novel exploration of machine learning solutions with supervised neural structures for nonlinear cholera epidemic probabilistic model with quarantined impact," *The European Physical Journal Plus*, vol. 140, no. 1, p. 64, 2025. View online.
- [6] A. H. Ali, A. Ahmad, F. Abbas, E. Hincal, A. Ghaffar, B. Batiha, and H. A. Neamah, "Modeling the behavior of a generalized cholera epidemic model with asymptomatic measures for early detection," *PloS One*, vol. 20, no. 3, p. e0319684, 2025. View online.
- [7] L. M. Anteneh, B. E. Lokonon, and R. G. Kakaï, "Modelling techniques in cholera epidemiology: A systematic and critical review," *Mathematical Biosciences*, p. 109210, 2024. View online.
- [8] C. H. Nkwayep, R. G. Kakaï, and S. Bowong, "Prediction and control of cholera outbreak: study case of cameroon," *Infectious Disease Modelling*, vol. 9, no. 3, pp. 892–925, 2024. View online.

- [9] J. Wang, "Mathematical models for cholera dynamics—a review," *Microorganisms*, vol. 10, no. 12, p. 2358, 2022. View online.
- [10] M. A. Ovi, A. Afilipoaei, and H. Wang, "Estimating hidden cholera burden and intervention effectiveness," *Bulletin of Mathematical Biology*, vol. 87, no. 6, pp. 1–30, 2025. View online.
- [11] A. A. Avwerosuo and A. M. Okedoye, "Mathematical modelling of the dynamics and control of communicable diseases with emphasis on cholera epidemics," *Asian Journal of Applied Science and Technology (AJAST)*, vol. 7, no. 4, pp. 99–119, 2023. View online.
- [12] R. C. Ratnayake, Case-Area Targeted Intervention for the Control of Cholera Epidemics in Crises: From Spatial Mathematical Modelling to Field Evaluation. PhD thesis, London School of Hygiene & Tropical Medicine, 2024. View online.
- [13] C. Trevisin, J. C. Lemaitre, L. Mari, D. Pasetto, M. Gatto, and A. Rinaldo, "Epidemicity of cholera spread and the fate of infection control measures," *Journal of the Royal Society Interface*, vol. 19, no. 188, p. 20210844, 2022. View online.
- [14] I. Ahmed, A. Akgül, F. Jarad, P. Kumam, and K. Nonlaopon, "A caputo-fabrizio fractional-order cholera model and its sensitivity analysis," *Mathematical Modelling and Numerical Simulation with Applications*, vol. 3, no. 2, pp. 170–187, 2023. View online.
- [15] S. Rashid, F. Jarad, and A. K. Alsharidi, "Numerical investigation of fractional-order cholera epidemic model with transmission dynamics via fractal–fractional operator technique," *Chaos, Solitons & Fractals*, vol. 162, p. 112477, 2022. View online.
- [16] Z. Shah, N. Ullah, R. Jan, M. H. Alshehri, N. Vrinceanu, E. Antonescu, and M. Farhan, "Existence and sensitivity analysis of a caputo-fabirizo fractional order vector-borne disease model," *European Journal of Pure and Applied Mathematics*, vol. 18, no. 2, pp. 5687–5687, 2025. View online.
- [17] M. Farman, R. Sarwar, K. S. Nisar, P. A. Naik, S. Shahzeen, and A. Sambas, "Global wave analysis of a fractional-order cholera disease model in society," *Network Modeling Analysis in Health Informatics and Bioinformatics*, vol. 14, no. 1, p. 15, 2025. View online.
- [18] A. Ahmad, F. Abbas, M. Farman, E. Hincal, A. Ghaffar, A. Akgül, and M. K. Hassani, "Flip bifurcation analysis and mathematical modeling of cholera disease by taking control measures," *Scientific Reports*, vol. 14, no. 1, p. 10927, 2024. View online.
- [19] M. L. Alhaji, F. A. Abdullah, and S. N. A. Mansor, "Application of the laplace-adomian decomposition method to the dynamics of cholera transmission," in *American Institute of Physics Conference Series*, vol. 3189, p. 030015, 2024. View online.
- [20] A. O. Yunus and M. O. Olayiwola, "The analysis of a co-dynamic ebola and malaria transmission model using the laplace adomian decomposition method with caputo fractional-order," *Tanzania Journal of Science*, vol. 50, no. 2, pp. 224–243, 2024. View online.
- [21] K. A. Bashiru, M. K. Kolawole, T. A. Ojurongbe, H. O. Adekunle, N. O. Adeboye, and H. A. Afolabi, "Conceptual analysis of a fractional order epidemic model of measles capturing logistic growth using laplace adomian decomposition method," *Journal of Applied Computer Science & Mathematics*, vol. 17, no. 35, 2023. View online.
- [22] P. B. Dhandapani, V. Leiva, C. Martin-Barreiro, and M. Rangasamy, "On a novel dynamics of a sivr model using a laplace adomian decomposition based on a vaccination strategy," *Fractal and Fractional*, vol. 7, no. 5, p. 407, 2023. View online.
- [23] M. K. Kolawole, "Mathematical dynamics of the (sveitr) model, the impact of treatment and vaccination on cholera spread," *Jurnal Diferensial*, vol. 7, no. 1, pp. 85–105, 2025. View online.
- [24] J. Adedeji and M. O. Olayiwola, "On analysis of a mathematical model of cholera using caputo fractional order: On analysis of a mathematical model of cholera," *Journal of the Nigerian Mathematical Society*, vol. 43, no. 3, pp. 287–309, 2024. View online.
- [25] A. Ghosh, P. Das, T. Chakraborty, P. Das, and D. Ghosh, "Developing cholera outbreak forecasting through qualitative dynamics: Insights into malawi case study," *Journal of Theoretical Biology*, vol. 605, p. 112097, 2025. View online.

- [26] E. O. Adeniyi, "Transmission dynamics and control of cholera in africa: A mathematical modelling approach," *unpublished manuscript*, 2024. View online.
- [27] J. Mushanyu, L. Matsebula, and F. Nyabadza, "Mathematical modeling of cholera dynamics in the presence of antimicrobial utilization strategy," *Scientific Reports*, vol. 14, no. 1, pp. 1–22, 2024. View online.
- [28] I. E. Onwunta, G. O. Ozota, C. A. Eze, I. F. Obilom, O. C. Okoli, C. N. Azih, and E. L. Agbo, "Recurrent cholera outbreaks in nigeria: A review of the underlying factors and redress," *Decoding Infection and Transmission*, vol. 3, p. 100042, 2025. View online.
- [29] O. B. Ojo and A. M. Gbolahan, "Contextualising cholera in nigeria: Contemporary epidemiology, determinants and recommendations," *ISA Journal of Medical Sciences (ISAJMS)*, vol. 2, no. 3, pp. 57–68, 2025. View online.
- [30] M. Oweibia, T. Egberipou, T. R. Wilson, G. C. Timighe, and P. D. Ogbe, "Factors associated with the propagation of cholera in epidemics across the geopolitical zones of nigeria: A systematic review," *medRxiv*, pp. 2025–05, 2025. View online.
- [31] S. Eneh, F. Onukansi, C. Anokwuru, O. Ikhuoria, G. Edeh, S. Obiekwe, and C. Okpara, "Cholera outbreak trends in nigeria: policy recommendations and innovative approaches to prevention and treatment," *Frontiers in Public Health*, vol. 12, p. 1464361, 2024. View online.
- [32] H. Yu, G. Cai, and Y. Li, "Dynamic analysis and control of a new hyperchaotic finance system," *Nonlinear Dynamics*, vol. 67, no. 3, pp. 2171–2182, 2012. View online.

Citation IEEE Format:

M. K. Kolawole and A. A. Adeniji. "Modelling Immunological Effects on Fractional Order of Cholera Dynamics with Behavioral Response via Numerical simulation", Jurnal Diferensial, vol. 7(2), pp. 190-214, 2025.

This work is licensed under a Creative Commons "Attribution-ShareAlike 4.0 International" license.

